1 November 2000

ELSEVIER

Optics Communications 185 (2000) 83–93

OPTICS COMMUNICATIONS

www.elsevier.com/locate/optcom

Operation of scanning plasmon near-field microscope with gold and silver tips in tapping mode: demonstration of subtip resolution

V.N. Konopsky *

Institute of Spectroscopy, Russian Academy of Sciences, Troitsk, Moscow region 142190, Russian Federation

Received 10 May 2000; received in revised form 8 August 2000; accepted 6 September 2000

Abstract

We present a scanning plasmon near-field microscope which operate in tapping mode of atomic force microscope. We interpret the observed maximum in light scattering intensity during a tip approach to (and withdrawal from) a surface as an electromagnetic (em) resonance in a tip–surface (sphere–plane) structure. This em resonance is of greater intensity when the tip and the surface are noble metals. At the em resonance in such a structure, the dimension of the light field localization is of the order of $L \simeq (2dR)^{1/2}$, where d is the tip–surface distance and R is the tip radius. Therefore at $d \ll R$ the resolution of the near-field images is less than tip radius ($L < R$). We propose to record the light signal at the second harmonic of tapping frequency to pick out the signal associated with the sphere–plane em resonance. Different registration modes of the light signal are considered and the nature of negative contrast of surface hillocks in certain of the registration modes is analyzed. Near-field images of rough silver surfaces are presented and it is shown that distribution of the near-field intensity on the surface is the result of the interference between scattering plasmons and the initial plasmon beam. © 2000 Published by Elsevier Science B.V.

PACS: 07.79.Fc; 61.16.Ch; 73.20.Mf

Keywords: Near-field optics; Surface plasmons; Apertureless scanning near-field optical microscopy; Plasmon resonances in tip-surface structure; Subtip resolution

1. Introduction

Near-field microscopy makes it possible to overcome Abbe's diffraction limit of conventional far-field optical microscopy [1–4]. At present, "standard" scanning near-field optical microscopes (SNOMs) employ aluminum-coated optical fibers tapered at their end as subwavelength light source. The smallest aperture that can be made at the very end of the aluminum-coated fiber cannot be much smaller than twice the optical skin depth in aluminum (skin depth ≃12 nm at 633 nm wavelength). Thus, typical lateral spatial resolutions achieved in SNOM are in the 30–50 nm range. Moreover, aperture-based SNOM often suffers from reduced optical power which can be delivered through the subwavelength aperture.

* Fax: +7-095-334-0886.

E-mail address: konopsky@isan.troitsk.ru (V.N. Konopsky).

0030-4018/00/$ - see front matter © 2000 Published by Elsevier Science B.V.
PII: S0030-4018(00)00994-9

In apertureless scanning near-field optical microscope (aSNOM) a sharp tip of a scanning tunneling microscope (STM) or atomic force microscope (AFM) is illuminated from the outside by an external light source and scatters the evanescent field which is then far-field detected [5]. The lateral resolution of aSNOM is determined by the tip size and reaches the value of 17–20 nm [6,7]. Without doubt there is a strong interest to push this limit further to the 1 nm scale in order to obtain information about optical properties at molecular resolution.

Even in the early proposals about aSNOM [8,9] the importance was pointed out of the excitation of the electromagnetic (em) resonance in a metalized tip, which is considered as a small particle (sphere or elongated ellipsoid). For better excitation of the em resonance in the visible region, the noble metal tip must be used. In these proposals the lateral resolution of such aSNOM is also anticipated to be about the dimension of the tip.

In this paper we develop an approach, which enables to reach the resolution less than the tip radius of aSNOM. The central idea is to use the em resonance in a tip–surface (sphere–plane) structure where tip and surface are the noble metals. The dimension of em field localization in such a structure at the em resonance is less than the radius of the curvature of the tip.

Partially such experimental situation is realized, for example, in scanning plasmon near-field microscopes (SPNMs) [10–16] where traveling surface plasmon field on the *silver* surface (which is important) is used as an external excitation source of aSNOM tip. Specht et al. in Ref. [10] reported that ultrahigh lateral resolution (3 nm) was reached. We will return to this work when we will discuss the distance dependence of the light scattering intensity in our setup.

The plan of this paper is as follows: Section 2 gives an account of the main features of the em resonance in sphere–plane structure, Section 3 describes our experimental setup and different registration modes of the light signal, Section 4 presents our experimental results and discussion and Section 5 is the conclusions.

2. The electromagnetic resonance in a sphere–plane structure

The em resonance in a sphere–plane structure was thoroughly studied in the early 80s in the context of light emission from small particle tunnel junctions [17,18], and in context of surface-enhanced Raman scattering [19]. For a detailed consideration of this subject one can see these excellent works, but we shall confine our account to a purely qualitative discussion of the problem.

An isolated small metal sphere with radius $R \ll \lambda$ and permittivity $\epsilon_2 = \epsilon_2' + i\epsilon_2''$ has an em resonance at the Frölich frequency ω_F, that is at the frequency where $\epsilon_2'(\omega_F) = -2\epsilon_0$ and $\epsilon_2''(\omega_F) \approx 0$ (ϵ_0 is the real permittivity of the environment). For metal particle with the permittivity given by the Drude's model, $\omega_F = \omega_p/(1+2\epsilon_0)^{1/2}$, where ω_p is the plasma frequency of electrons (see, for example, Ref. [20]). When the sphere approaches a metal surface an interaction between the Frölich mode of the sphere (i.e. localized plasmon) and an eigenmode of an em excitation of a metal–dielectric interface (i.e. surface plasmon) takes place. This interaction shifts the Frölich mode frequency in the lower frequency region. When the distance between the metal sphere and the metal plane becomes small ($d \ll R$) these original resonance modes are so strongly distorted by their mutual interaction that the excitation spectrum of the sphere–plane structure cannot be classified in terms of the original, noninteracting resonances. Because of this the resonances in the sphere–plane structure at $d \ll R$ are often called "gap modes". The eigenfrequencies of these modes may be determined from the next approximated analytical expression [21]:

$$\frac{\epsilon_0}{\epsilon_1'(\omega)} + \frac{\epsilon_0}{\epsilon_2'(\omega)} = -\left(n + \frac{1}{2}\right)\sqrt{\frac{2d}{R}}, \quad n = 0, 1, 2, \ldots, \tag{1}$$

where $\epsilon_2'(\omega)$ and $\epsilon_1'(\omega)$ are the real parts of the permittivities of the sphere and the plane. In our configuration (see Fig. 1a) $\epsilon_2'(\omega)$ and $\epsilon_1'(\omega)$ are the real parts of the permittivities of a tip and a surface, R is a radius of curvature of the tip and d is a distance between the tip and the surface. Therefore

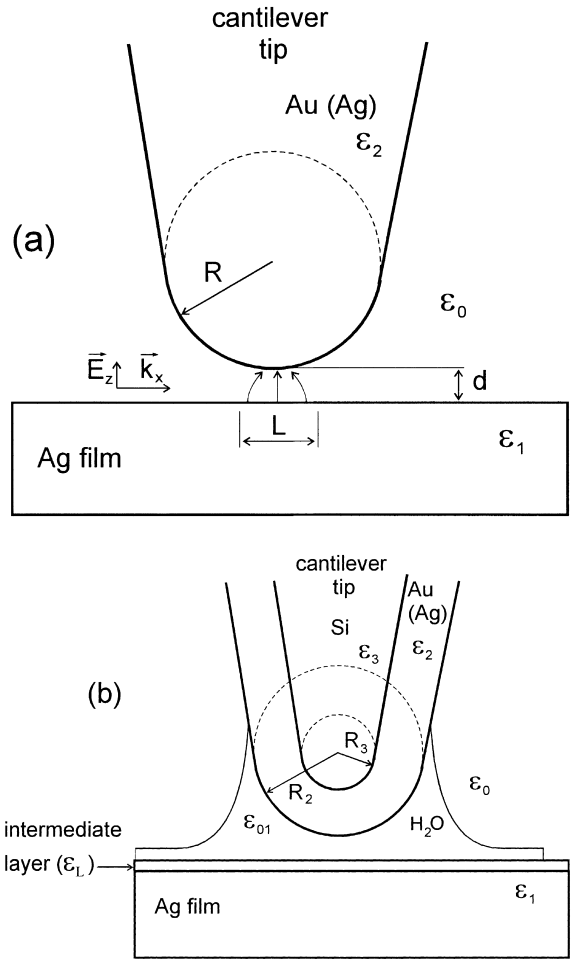

Fig. 1. (a) Tip–surface structure considered in theoretical calculations, and (b) one in a real experimental situation.

if we will excite the gap between the needle and the surface by an em radiation with a fixed frequency (e.g. by He–Ne laser) the em resonance in this sphere–plane structure occurs at the next "resonance" distance between tip and surface:

$$d_{\mathrm{res}} = 2R\left[\frac{\epsilon_0}{\epsilon_1'(\omega_{\mathrm{He\text{–}Ne}})} + \frac{\epsilon_0}{\epsilon_2'(\omega_{\mathrm{He\text{–}Ne}})}\right]^2 \qquad (2)$$

(hereinafter we shall consider "gap mode" with $n = 0$). In other words an "effective" dipole moment of the sphere–plane structure has a maximum amplitude at $d = d_{\mathrm{res}}$, and it decreases when the tip approaches the surface at the distance $d < d_{\mathrm{res}}$ and moves away from the surface at the distance $d > d_{\mathrm{res}}$. Notice also that the presence of intermediate layers with $\epsilon_0 > 1$ has a pronounced effect on d_{res} ($d_{\mathrm{res}} \sim \epsilon_0^2$).

The important characteristic feature of the sphere–plane em resonance is the lateral dimension L of the em field localization between the sphere and the plane. It is approximately equal [17,18,21]:

$$L \approx \sqrt{2dR}. \qquad (3)$$

Therefore at $d \ll R$ this dimension is less than tip radius ($L < R$). As a result a huge increase of the light intensity under the sphere takes place [18,19].

It is obvious that the tip of SPNM will scatter the surface plasmons more effectively when it is placed at the distance d_{res} from the surface. If we will modulate the tip–surface distance at a frequency Ω, then we can pick out the signal associated with sphere–plane resonance by detecting a light signal at the frequency 2Ω. The lateral resolution of the light signal detected at the second harmonic of the tip oscillation will be of the order of L.

3. Experimental setup

Fig. 2 is a schematic of our experimental setup. A beam of a cw He–Ne laser ($\lambda = 632.8$ nm, $I \simeq 1$ mW), incident on a silver film with thickness 50 nm (which was thermally evaporated on the base of a quartz prism) at a defined angle θ_0 of total internal reflection, excites the surface plasmons at the silver–air interface (it is usual Kretschmann configuration).

The excitation of the surface plasmons can be recognized by a minimum in the reflected laser intensity which can be understood as destructive interference between light reflection from the silver–air and silver–quartz interfaces [22]. A commercial scanning probe microscope "Solver P-47" of "NT-MDT" firm [23] with gold and silver coated silicon cantilevers has been used in common AFM mode (a bend of the cantilever is held constant by AFM feedback during scan) and in

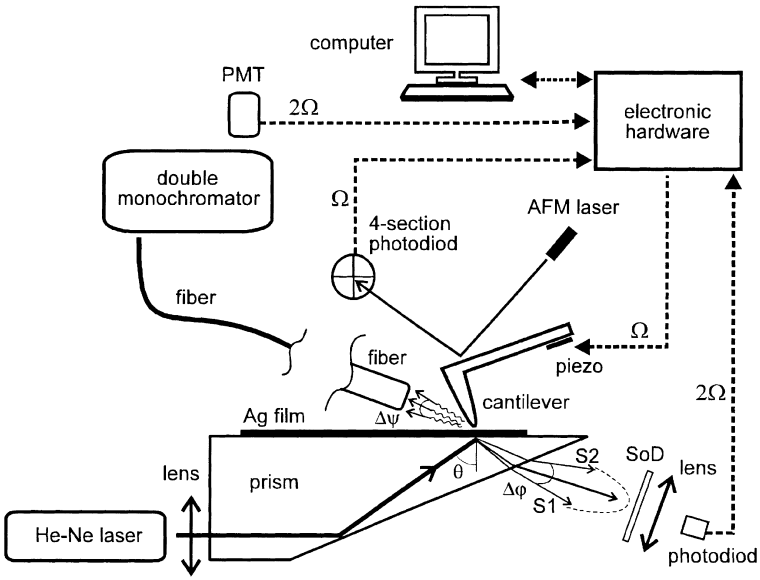

Fig. 2. Schematic of the experimental setup: PMT – photo-multiplier tube, SoD – set of diaphragms; scattered rays S1–S2 and angle $\Delta\varphi$ between them lie in the plane which is perpendicular to the plane of the figure.

tapping mode of AFM (an amplitude of the cantilever vibration is held constant by AFM feedback during scan).

Several registration modes of the light signal are used in our setup.

1. *Internal reflection registration mode* – it is the registration of the intensity variation of the reflected light beam. (Scattered light rays (S1–S2) are removed by the set of diaphragms – SoD.) This registration mode is the one that was used in the works [10,11],
2. *Internal scattering registration mode* – it is the registration of the intensity of the conical light radiation arisen from elastic scattering of the surface plasmons in the angle $\Delta\varphi$ between rays S1 and S2 (reflected light beam is removed by the set of diaphragms – SoD). This registration mode is similar to the one that was used in the works [12–15], but in these works the overall conical light radiation was collected by a cylindrical mirror (i.e. $\Delta\varphi = 2\pi$ in these works; in our case $\Delta\varphi \simeq 23°$).
3. *External scattering registration mode* – it is the registration of the plasmon–photon scattering using the multimode fiber with diameter 300 μm and numerical aperture ≈0.4 placed in the immediate vicinity (0.5 mm) of the cantilever tip. Undesirable scattered light from AFM laser diode ($\lambda \simeq 670$ nm) has been removed by double monochromator. The light signal has been detected by a photo-multiplier tube (PMT) placed on the exit of double monochromator.

In each mentioned above registration modes the light signal can be recorded:

(a) *without modulation*: that is AFM operates in the common mode and light signal is detected at zero frequency;

(b) *at the first harmonic of the cantilever vibration*: that is AFM operates in the tapping mode and light signal is detected at a frequency Ω of a cantilever vibration;

(c) *at the second harmonic of the cantilever vibration*: that is AFM operates in the tapping mode and light signal is detected at a frequency 2Ω.

A typical value of the resonant frequency of gold- and silver-coated cantilevers in our setup was $\Omega \approx 40$ kHz. The amplitude of the cantilever vibration was about 150 nm, and it was kept constant by AFM feedback during the scan.

4. Experimental results and discussion

4.1. Distance-dependent variation of the light signal

To understand the advantages of the light registration at the second harmonic of the tip–surface distance modulation one must consider the variation of the light signal while the tip–sample distance is varied. The distance-dependent intensity of the light signal in the "external scattering registration mode" is presented in Fig. 3. A gold-coated silicon tip with $R \simeq 190$ nm (see Section 4.2) is used to obtained this dependence. One can see that light intensity decreases during the tip withdrawal from the surface, but some maximum ("bump") takes place at the curve at $x = 35$ nm.

Similar "bumps" were also detected by other authors in different registration modes of SPNM. See, for example, Refs. [10,16] ("internal reflection registration mode") and also Ref. [12] ("internal scattering registration mode"), but we have found that in the "external scattering registration mode" this maximum is more pronounced. A strong narrow peak of the light scattering intensity was also observed in the work [24], when a gold-coated polystyrene particle is approached to a sample surface, but the experimental situation in this work differs from the one in the SPNM. To the best of our knowledge, only the work [10] gives some discussion about the origin of the maximum on the distance-dependent intensity of the SPNM light signal. Specht et al. considered the tip as an oscillating dipole immersed in the "driving" em field and claimed that the strong decrease of light intensity on a short distance from the metal surface is the result of the radiationless energy transfer from the tip ("dipole") to the metal surface. Specht et al. also believed that it is the mechanism of radiationless energy transfer which is responsible for ultrahigh resolution (3 nm) in their setup.

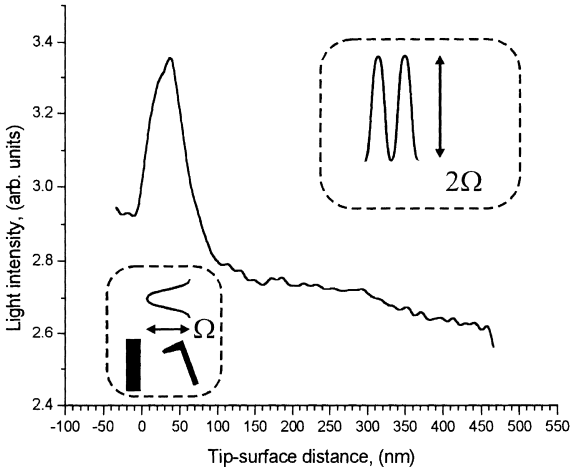

Fig. 3. The distance-dependent intensity of the light signal in "external scattering registration mode". On insets in dashed-line frames the mechanism of the 2Ω frequency generation at the tip–surface distance modulation by Ω frequency is illustrated.

We believe that our model of the sphere–plane em resonance is more adequate in this case (in other words we think that one must consider the dipole moment of the tip–surface system taken as a whole, but not the isolated dipole moment of the tip). Though we must note that in our model radiationless energy losses are also very important, especially for ultrasharp tips (Specht et al. used tungsten tips with radii of curvature about 10 nm). For ultrasharp tips, and as a consequence at ultrasmall dimension L of the localization of the em field under tip (see Eqs. (3) and (2)), the process of generation of electron–hole pairs by the short-wavelength Fourier component of the em field ($k_{\mathrm{em}} \sim 1/L$) becomes the main damping mechanism of the sphere–plane em resonance. The decay time of the em resonance in this case is [25]

$$\frac{1}{\tau} \approx \frac{1}{2}\frac{v_{\mathrm{F}}}{L}, \tag{4}$$

where v_{F} is the Fermi's velocity of electrons in a metal ($v_{\mathrm{F}} \simeq 1.4 \times 10^8$ cm/s for Au and Ag). Increasing of the absorption of the em radiation by the tip–surface structure (when ultrasharp tips are used) becomes important at comparison of signal/noise ratios of different registration modes.

Returning to Fig. 3 one can see on insets in dashed-line frames the elucidation of the mechanism of the 2Ω frequency generation at the tip–surface distance modulation by Ω frequency. It is clear that the light signal at 2Ω frequency associated with the sphere–plane em resonance will have the lateral resolution about L.

4.2. Determination of the radii of the tips

For quantitative comparison of the Eq. (2) with experiment we must know the radii of the tips used in our setup. For this purpose we used a commercial test grating TGT 01 of the "NT-MDT" firm [23]. This test grating is the set of ultrasharp silicon needles with radii of curvature $r \approx 10$ nm. Radii of curvature of images of these needles R^* is $R^* = r + R$, where R is the radius of the cantilever tip that was used to obtain the image. Our experiments with ultrasharp "Park Scientific Instruments" cantilevers have shown that needles of the test grating TGT 01 are actually ultrasharp. We obtain the value $R^* \approx 30$ nm from these experiments and we get conclusion that r of the test needles lies in the range $r \simeq 10$–15 nm.

Typical image of the test grating TGT 01 is given in Fig. 4a (gold-coated silicon cantilever was used). From cross-section of a needle (see Fig. 4b) one can see that $R^* \simeq 200$ nm, and therefore our gold-coated cantilever tips have the radii of curvature $R_{\mathrm{Au}} \simeq 185$–$190$ nm. From analogous images we get the conclusion that our silver-coated cantilever tips have the radii of curvature $R_{\mathrm{Ag}} \simeq 150$ nm, and that our uncoated silicon tips have the radii of curvature $R \simeq 85$–100 nm.

Now, using the Eq. (2) with $R_{\mathrm{Au}} \simeq 190$ nm, $\epsilon_{\mathrm{Ag}} \simeq -18$, $\epsilon_{\mathrm{Au}} \simeq -12$ at $\lambda = 632.8$ nm [26] and $\epsilon_0 = 1$ we obtain $d_{\mathrm{res}} \simeq 8$ nm. But from Fig. 3 one can see that experimental value $d_{\mathrm{res}} \simeq 35$ nm. We assume that this discrepancy is due to differences between the real experimental situation (schematically shown on the Fig. 1b) and idealized situation (schematically shown on the Fig. 1a) that was used to obtain the Eqs. (1) and (2). We believe that the presence of intermediate layers on the silver surface in the air (chiefly silver sulfide tarnish layer [27]: $\varepsilon'_{\mathrm{Ag_2S}} = 8.7$ and adsorbed water: $\varepsilon'_{\mathrm{H_2O}} = 1.8$) may account for this discrepancy. From Eq. (2) one can see that d_{res} is strongly dependent on ϵ_0 ($d_{\mathrm{res}} \sim \epsilon_0^2$). For a good agreement with the observed value of d_{res} it is necessary that the "effective" permittivity of the media between the tip and the silver surface was about $\epsilon_0 \approx 2$. The presence of the silicon core in the tip and the fact that in our case $R < \lambda$, but not $R \ll \lambda$ may be of importance for this discrepancy as well.

4.3. Demonstration of the lateral resolution in our setup

In Fig. 5 one can see the topography (a) and optical signal (b) of some surface hillock on silver surface. Scan size is 700×700 nm^2. Optical signal was recorded at 2Ω frequency in the "internal scattering registration mode" (i.e. $2c$ mode in our notation, see Section 3). Reasons for the common *negative contrast* of near-field images of surface hillocks in this registration mode will be discussed in the Section 4.5. On the Fig. 5c and d one can see cross-sections of the 5a and b images correspondingly, taken at $x \simeq 150$ nm (designated by arrows on 5a and b images). From these cross-sections we get conclusion that the lateral resolution of near-field images in our setup lies in the range $\simeq$50–70 nm. One can see that this resolution is less than radius of curvature of our tip ($R \simeq 190$ nm). From Eq. (3), using experimental value of $d_{\mathrm{res}} \simeq 35$ nm one can obtain the dimension of the light field localization $L = 115$ nm. Resolution is determined by the light intensity (that is by the square of the light field) and it is better than L.

4.4. Distribution of the near-field intensity of the surface plasmons on rough silver surface: interference between scattering plasmons and initial plasmon beam

Fig. 6b illustrates the distribution of the near-field intensity of the surface plasmon field on a silver surface (direction of the initial surface plasmon beam designated by the arrow). Scan size is 8810×8810 nm^2. Optical signal was recorded at 2Ω frequency in the "internal scattering registration mode" (i.e. $2c$ mode). From mathematical data processing of the topography of this part of surface (Fig. 6a) we obtain the root-mean-square height of the surface roughness $\delta = \langle (\Delta z)^2 \rangle^{1/2} \simeq 5.1$ nm.

The comparison of the surface topography (Fig. 6a) and near-field (Fig. 6b) images reveals two main features:

1. There is a correlation between the two images, i.e. the hillocks on the surface topography correspond to the white spots on the near-field image.

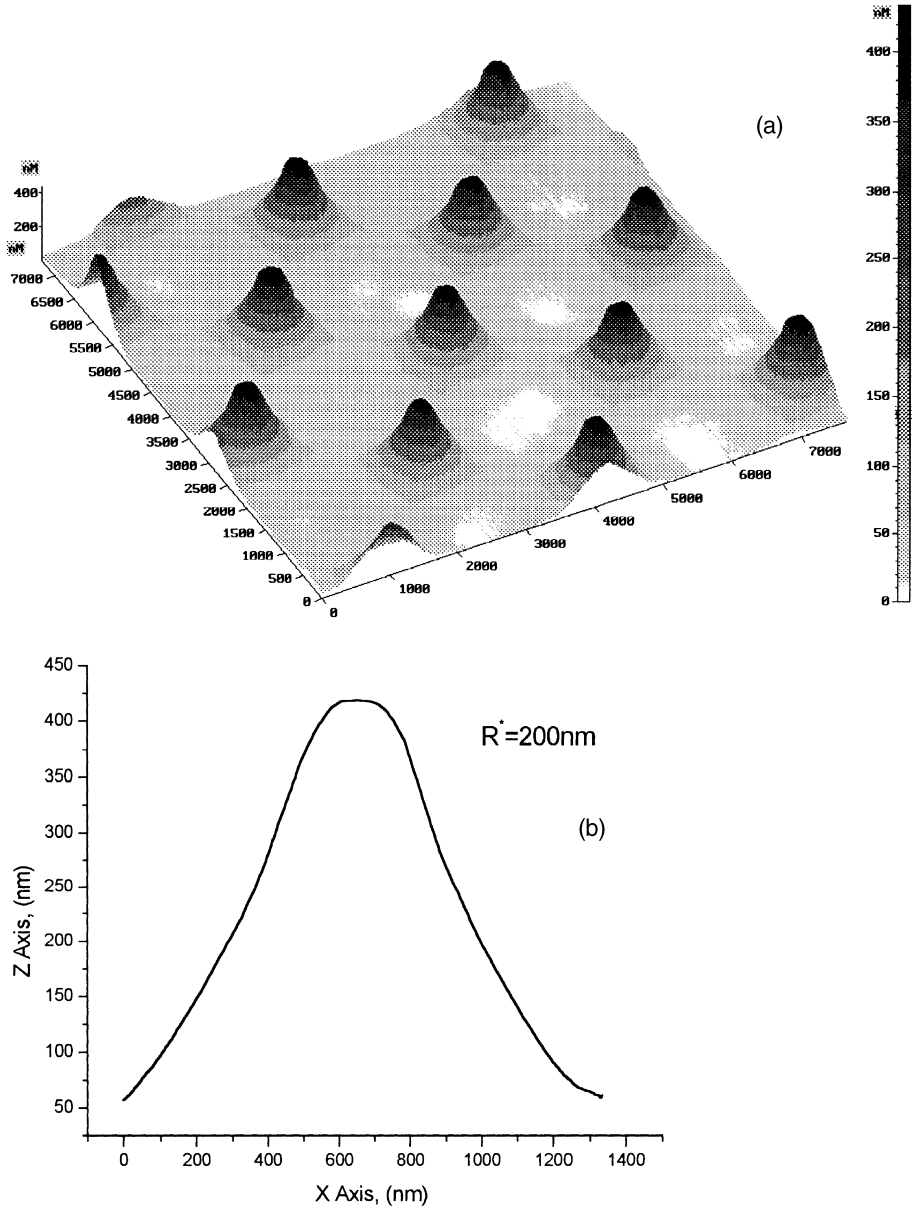

Fig. 4. (a) AFM image of the test grating TGT 01 obtained using gold-coated silicon cantilever. (b) Cross-section of one needle.

2. Apart from that, some additional structure (ripples and fringes) is appearing on the near-field images.

Similar near-field pictures have been observed by other authors using SPNM (see, for instance Refs. [10,12–14]) and SNOM [28]. But to our knowledge, the reasons of appearance of such "cluster structure" of an em field which is not associated with any particular features in the surface topography have not been clearly illuminated. To attain such an understanding one must perform the fast Fourier transformation (FFT) of the near-field

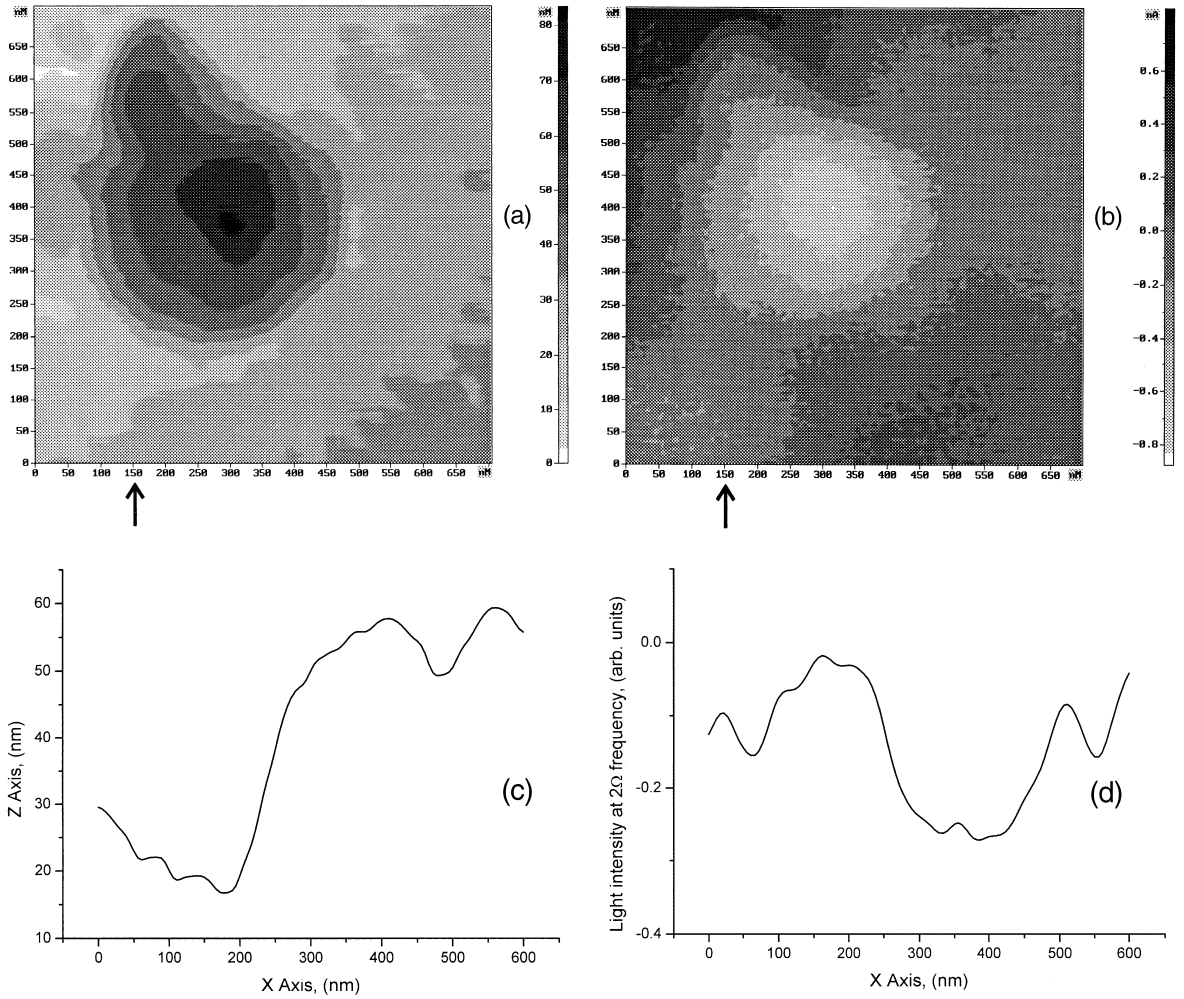

Fig. 5. (a) AFM and (b) SPNM images of some surface hillock on silver surface (scan size is 700×700 nm^2). (c) and (d) are cross-sections of the (a) and (b) images correspondingly, taken at $x \simeq 150$ nm (designated by arrows at (a) and (b) images).

image. In Fig. 6d one can see a distinct circle in the FFT of the near-field image (the second circle arises because of inherent feature of Fourier transformation: a FFT image is symmetric respective to the origin of the coordinates). The explanation of the appearance of such a circle in the FFT image is given in Fig. 6c. The initial surface plasmon beam is scattered by the surface roughness and interference between initial surface plasmon beam and scattering plasmons takes place. At elastic scattering the wave vector of the initial plasmon $\mathbf{k}_{\mathrm{pl}}$ changes its direction, but its magnitude remains the same ($|\mathbf{k}_{\mathrm{pl}}| = |\mathbf{k}_{\mathrm{sc}}|$). The distribution of the SP near-field intensity on the surface is $I_{\mathrm{pl}} + I_{\mathrm{sc}} + 2\sqrt{I_{\mathrm{pl}} I_{\mathrm{sc}}} \cos((\mathbf{k}_{\mathrm{pl}} - \mathbf{k}_{\mathrm{sc}})\mathbf{r})$. So the "vectors of the interference gratings" $\mathbf{K}_{\mathrm{int}} = \mathbf{k}_{\mathrm{pl}} - \mathbf{k}_{\mathrm{sc}}$ are distributed so that their ends lie on the circle with radius equals $|\mathbf{k}_{\mathrm{pl}}|$. One can see from the FFT image that forward scattering (small $\mathbf{K}_{\mathrm{int}}$) is of the greatest intensity. The angular dependence of the surface plasmon scattering by surface roughness is of great concern, for example, in studies of laser damage of metal mirrors. The surface plasmons play a crucial role in such a damage [29] and

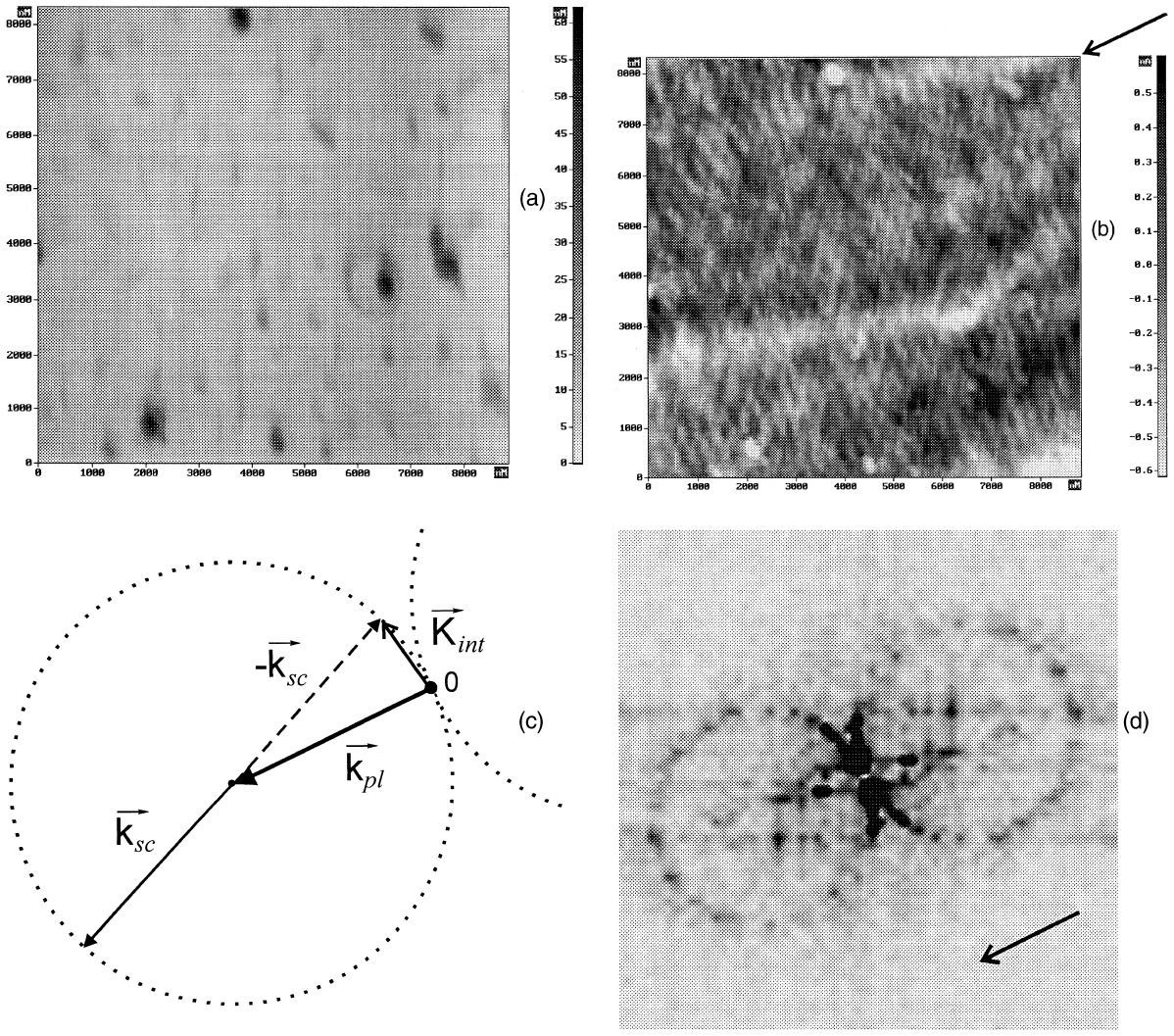

Fig. 6. (a) AFM and (b) SPNM images of silver surface (scan size is 8810×8810 nm^2). (d) is FFT of SPNM image (the arrow length on FFT image corresponds to the surface plasmon wave vector length $|\mathbf{k}_{pl}|$) and (c) is the schematic of the interference of surface plasmons.

elimination of the surface plasmons caused by the surface roughness is of considerable importance for increasing the laser damage threshold of metal mirrors [30]. But for quantitative analyzes of plasmon scattering by FFT of near-field images it is better to use "internal reflection registration mode" or "internal scattering registration mode" in which the overall conical light radiation is collected by a cylindrical mirror (like it was done in Refs. [12–15]), because a nonuniformity in the registration of the scattered light leads to some artifacts in near-field images. These questions will be considered in detail elsewhere [31].

It must be also noted that for very large surface hillocks (when the cross-section of surface plasmon scattering of a large hillock and the one of the tip becomes comparable in magnitude) the effects of multiple scattering are important. In this case typical V-shaped figures near the large point-like hillock occur in the SPNM image. The explanation

of this effect can be found in Ref. [15]. Other effects of the multiple scattering such as backscattering enhancement of surface plasmons have been also observed on specific surfaces [31].

4.5. Nature of the negative contrast of the surface hillocks in the "internal scattering/reflection registration modes"

The nature of the *negative contrast* in the SPNM images of the surface hillocks, as far as we know, has not been yet clearly illuminated. Indeed, one can expect an increasing of the em field at a hillock while we (and other authors) observed the negative contrast of the surface hillocks in "internal scattering registration mode" and in "internal reflection registration mode", whereas we have found that in "*external scattering registration mode*" the surface hillocks display the *positive contrast*. To explain such a property of SPNM images one must recall how near-field images are produced in these registration modes.

In "internal scattering registration mode" the AFM tip causes the *elastic* scattering of the *traveling* surface plasmons. And only plasmons with $|\mathbf{k}_{sc}| = |\mathbf{k}_{pl}|$ transfer to the conical em radiation which is then detected. But above a hillock there are no *traveling* surface plasmons, which can be elastically scattered by the tip. Whereas the strong em field above a hillock it is the field of the *localized* surface plasmons (with $|\mathbf{k}_{local}| \neq |\mathbf{k}_{pl}|$).

An analogous situation takes place in "internal reflection registration mode", where elimination of *traveling* surface plasmons, which would transfer to the photons and destructively interfere with the light reflected from the silver–quartz interface is the cause of the SPNM signal.

In other words in these two modes SPNM displays the intensity distribution of only *traveling* plasmons on the surface.

5. Conclusions

In this paper a scanning plasmon near-field microscope operating in tapping mode of AFM was presented. The gold- and silver-coated cantilevers were used to enhance an em resonance in a tip–surface (sphere–plane) structure. At the em resonance in such a structure, the dimension of the light field localization is of the order of $L \simeq (2dR)^{1/2}$, where d is the tip–surface distance and R is the tip radius. Therefore at $d \ll R$ the resolution of the near-field images is less than the tip radius ($L < R$). We came to the conclusion that a maximum on a curve of the distance-dependent optical signal intensity is the result of the em resonance in the tip–surface structure. We have recorded the optical signal at the second harmonic of tapping frequency to pick out the signal associated with the sphere–plane em resonance. It was shown that the optical resolution in our setup indeed is better than tip radius. Near-field images of rough silver surfaces have been presented and it has been shown that the distribution of the near-field intensity on the surface is the result of the interference between scattering plasmons and the initial plasmon beam.

Acknowledgements

The author thanks N.N. Novikova and Y.E. Petrov for silver coating of cantilevers and prisms, K.E. Kouyanov for technical assistance at work with electronic hardware and A.M. Lifshits for supply of optical fibers. The present research was supported by RFFI grant no 98-02-17206a and by programs "Fundamental spectroscopy" and "Fundamental metrology" of Russian Ministry of Science.

References

[1] E.H. Synge, Philos. Mag. 6 (1928) 356.
[2] E.A. Ash, G. Nicholls, Nature 237 (1972) 510.
[3] D.W. Pohl, W. Denk, M. Lanz, Appl. Phys. Lett. 44 (1984) 651.
[4] E. Betzig, J.K. Trautman, T.D. Harris, J.S. Weiner, R.L. Kostelak, Science 251 (1991) 1468.
[5] F. Zenhausern, M.P. O'Boyle, H.K. Wickramasinghe, Appl. Phys. Lett. 65 (1994) 1623.
[6] A. Lahrech, R. Bachelot, P. Gleyzes, A.C. Boccara, Opt. Lett. 21 (1996) 1315.
[7] R. Bachelot, P. Gleyzes, A.C. Boccara, Appl. Opt. 36 (1997) 2160.
[8] V.A. Namiot, Biofizika 30 (1985) 602 (in Russian).

[9] J. Wessel, J. Opt. Soc. Am. B 2 (1985) 1538.
[10] M. Specht, J.D. Pedarnig, W.M. Heckl, T.W. Hänsch, Phys. Rev. Lett. 68 (1992) 476.
[11] J.D. Pedarnig, M. Specht, W.M. Heckl, T.W. Hänsch, Appl. Phys. A 55 (1992) 476.
[12] Y.-K. Kim, P.M. Lundqist, J.A. Helfrich, J.M. Mikrut, G.K. Wong, P.R. Auvil, J.B. Ketterson, Appl. Phys. Lett. 66 (1995) 3407.
[13] Y.-K. Kim, J.B. Ketterson, D.J. Morgan, Opt. Lett. 21 (1996) 165.
[14] Y.-K. Kim, P.R. Auvil, J.B. Ketterson, Appl. Opt. 36 (1997) 841.
[15] P.R. Auvil, J.B. Ketterson, Y.-K. Kim, A. Kryukov, Appl. Opt. 37 (1998) 8448.
[16] J. Boneberg, M. Ochmann, H.-J. Münzer, P. Leiderer, Ultramicroscopy 71 (1998) 345.
[17] R.W. Rendell, D.J. Scalapino, B. Mühlschlegel, Phys. Rev. Lett. 41 (1978) 1746.
[18] R.W. Rendell, D.J. Scalapino, Phys. Rev. B 24 (1981) 3276.
[19] P.K. Aravind, H. Metiu, Surf. Sci. 124 (1983) 506.
[20] C.F. Bohren, D.R. Huffman, Absorption and Scattering of Light by Small Particles, Wiley-Interscience, New York, 1983.
[21] A.G. Mal'shukov, Phys. Rep. 194 (1990) 343.
[22] H. Raether, Surface Plasmons, Springer Tracts in Modern Physics, vol. 111, Springer, Berlin, 1988.
[23] http://www.ntmdt.ru.
[24] U.Ch. Fischer, D.W. Pohl, Phys. Rev. Lett. 62 (1989) 458.
[25] E.I. Ibragimov, A.G. Mal'shukov, Optika i Spektroskopia 76 (1994) 350 (in Russian).
[26] P.B. Johnson, R.W. Christy, Phys. Rev. B 6 (1972) 4370.
[27] J.M. Bennett, J.L. Stanford, E.J. Ashley, J. Opt. Soc. Am. 60 (1970) 224.
[28] J.R. Krenn, R. Wolf, A. Leitner, F.R. Aussengg, Opt. Commun. 137 (1997) 46.
[29] A.E. Siegman, P.M. Fauchet, IEEE J. Quant. Electron. QE-22 (1986) 1384.
[30] V.N. Konopsky, Opt. Laser Technol. 32 (2000) 15.
[31] V.N. Konopsky, K.E. Kouyanov, N.N. Novikova, unpublished.